Nanoscale Advances

ROYAL SOCIETY OF CHEMISTRY

PAPER

View Article Online
View Journal | View Issue

Cite this: *Nanoscale Adv.*, 2023, **5**, 4579

A Janus membrane doped with carbon nanotubes for wet–thermal management†

Boyang Tian, Miaomiao Hu, Yiwen Yang and Jing Wu *

In a human skin–fibrous fabric–external environment, fibrous materials, as the "second skin" of the human body, provide comfort against the wet and heat effectively. Fibrous materials protect human health and guarantee work efficiency in various outdoor or inner scenes. Personal wet–thermal management based on fibrous materials can regulate comfort in a facile manner with low or zero energy consumption, which has become a potential development area. However, realizing synergistic management of the wet and heat effectively and conveniently is a challenge in the development and production of fibrous materials. We designed and fabricated a Janus fibrous membrane composed of 3-(trimethoxysilyl)propyl methacrylate (TMSPMA)-modified hydrophobic cotton gauze and electrospun carbon nanotubes (CNTs)-doped cellulose acetate (CA) hydrophilic fibrous membrane. Taking advantage of asymmetric wettability along its thickness direction, the Janus fibrous membrane, acting as a "liquid diode", could transport sweat/moisture from human skin to the external environment unidirectionally, which endowed a dry surface on human skin, avoiding "stickiness", and realizing wet management. Doped CNTs had good photothermal-conversion capacity, so the Janus membrane exhibited excellent heating capacity for passive radiation, so excellent synergistic wet–thermal management was obtained. The Janus membrane could be a candidate for diverse applications of fibrous membranes. Our data provide new ideas for the design and fabrication of fibrous membranes with remarkable wet–thermal management.

Received 8th June 2023
Accepted 26th July 2023

DOI: 10.1039/d3na00398a

rsc.li/nanoscale-advances

Introduction

In humans, thermal management (*i.e.*, maintaining a constant body temperature and feeling neither too cold nor too hot) is a basic psychological and physiological need.[1,2] In some scenarios, especially in a cold environment, to maintain thermal comfort, various heating devices have been applied. Heating, ventilation, and air conditioning systems have been used widely, and have inevitably accounted for a huge proportion of global energy consumption (~47%).[3–5] However, with rapidly increasing populations, energy problems (*e.g.*, shortage of oil, electricity or other natural resources) and the global energy crisis have become more severe. In addition, with the burning of fuel during heating, the massive release of greenhouse gases (*e.g.*, CO_2, NO_2) will aggravate global warming, leading to serious environmental pollution and affecting sustainable development.[6,7] Accordingly, there is an urgent need to create a new strategy to realize the thermal comfort of humans with less energy consumption.[8–10]

As the "second skin" of the human body, the original function of clothing was to maintain a constant body temperature by adding or reducing the amount of clothes worn. The development of textiles has evolved along with human progress.[11,12] The development of new textiles by designers has increased the demand for clothing thanks to the introduction of innovative materials and improvement in techniques for making clothing.[13–17] Various applications of contemporary fabrics have been investigated. Regardless of how human civilization evolves, the primary and basic purpose of textiles will be to deliver thermal comfort and protection from water to the human body. Accordingly, by adjusting the ability of fabrics to absorb or reflect infrared light, the body can be kept at a comfortable temperature in cold environments, thereby improving work efficiency outdoors.[18,19] Conductive materials can also be added to the surface or inside of a fabric to achieve active heating.[20–22] However, a large proportion of clothing with heating capacity requires external power (*e.g.*, electric), which causes loss of energy as well as the comfort and portability of the textile itself. Therefore, thermal management of textiles with high efficiency and low energy consumption without sacrificing body comfort needs to be developed.

Carbon nanotubes (CNTs) are typical nanomaterials. CNTs have received extensive attention and research since their discovery by Iijima in 1991.[23] Usually, heat transfer in CNTs is considered to be dominated by phonon conduction. The regular

Beijing Key Laboratory of Clothing Materials R & D and Assessment, Beijing Engineering Research Center of Textile Nanofiber, School of Materials Design & Engineering, Beijing Institute of Fashion Technology, Beijing 100029, China. E-mail: a.wujing@163.com

† Electronic supplementary information (ESI) available. See DOI: https://doi.org/10.1039/d3na00398a

crystal structure and sp^2 structure of the carbon atom make phonon conduction favourable.[24,25] Thus, CNTs have extremely high axial thermal conductivity. It has been reported that the thermal conductivity of a single CNT ranges from 2000 to 6000 W m^{-1} K^{-1} depending on the type, size, and degree of purification of CNTs.[26–28] Due to the black appearance of CNTs, they absorb light thoroughly and have high efficiency for photothermal conversion. Thanks to such excellent thermal properties, CNTs have often been used for composite fillers to improve the thermal conductivity of polymers. Hu *et al.*[29] prepared an intrinsically flexible phase-change composite paraffin wax-styrene butadiene styrene/carbon nanotube (PW-SBS/CNT). In the day time, paraffin wax was in a melting state, absorbed solar energy, and stored it. At night, the liquid paraffin would change to a solid-state phase, and the stored heat during day time was released slowly. Due to the excellent photothermal-conversion ability of CNTs, the energy-storage efficiency of a designed energy-storage system can reach 85.93% at a light intensity of 175 mW cm^{-2}. Chen *et al.*[30] proposed an efficient and sustainable preparation method using laminated PET as raw material composite membranes with CNTs–MnO_2 nanowires on the outer layer and PET fibers@Ag on the inner layer. Such composite membranes could increase the surface temperature by 11.9 °C compared with the ordinary PET membrane. Zhang *et al.*[31] prepared graphite-welded CNTs/polydimethylsiloxane (w-CNTs/PDMS) polymer-based composites. If the content of w-CNTs was 4.57 wt%, the thermal conductivity of the PDMS/w-CNTs composite was as high as 13.1 W m^{-1} K^{-1}. Wang *et al.*[32] obtained covalently bonded cavernous CNTs in a three-stage tubular furnace, and permeated polyvinylidene difluoride (PVDF) into cavernous CNTs. If the filling mass fraction of CNTs was 21%, it increased four times compared with non-covalently bonded CNTs with a similar filling quantity.

For textiles, sweat/moisture removal (*i.e.*, water management) is also a guarantee for basic wearability and functionalization. Traditional textiles, such as cotton[33] and silk fabric,[34–37] can remove sweat by the wicking effect of fabric yarns. However, if the amount of sweat/moisture increases and exceeds the maximum amount absorbed, then the textile is saturated with sweat/moisture, clings to human skin, and makes people feel "sticky". Moreover, in extreme cold, if sweat cannot be drained out in a timely manner, it can make the human body much colder or even cause hypothermia. Textiles that can remove sweat quickly could have a key role in solving this problem. A Janus membrane with asymmetric wettability (*i.e.*, an asymmetric membrane with a lyophobic layer on one side and a lyophilic layer on the other side) has been explored as a "liquid diode" in which liquid can be transported from one side of a membrane to another side, but liquid transport in the reverse direction is blocked.[38–40] Such novel and unique liquid-driven capacity has attracted much attention, and shown potential applications in wet or wet–thermal management.[41,42]

We considered the synergistic effect of wetness and heat in the micro-environment of a human skin–fibrous fabric–external environment system. We proposed fabrication of a CNTs-doped Janus fibrous membrane with asymmetric wettability *via* facile chemical grafting and electrospinning. Addition of CNTs to a CA electrospinning solution followed by electrospinning was a facile and efficient way for fabrication of a CNTs@CA fibrous membrane. In addition, a hydrophobic layer was constructed using modified hydrophilic commercial gauze. Taking advantage of larger pores, the capacity for unidirectional liquid transport could be implemented, allowing sweat to be transported from the hydrophobic gauze to the external environment easily. Besides, the doped CNTs enhanced the photothermal-conversion performance and thermal conductivity of the Janus membrane, providing the possibility to maintain a consistent and optimal body temperature even in cold environments. Such a CNTs-doped Janus fibrous membrane could realize heat collection without extra energy consumption, thereby maintaining body temperature at a comfortable range and guaranteeing daily life and work. However, it could also improve unidirectional transport of sweat and moisture to improve wet comfort, which guarantees multiple functions of an "intelligent" wearable fabric.

Experimental section

Materials

Cotton gauze (Beijing, China) was used after cleaning with ethanol under sonication. 3-(Trimethoxysilyl)propyl methacrylate (TMSPMA, 98%), cellulose acetate (CA, M_n = 50 000), and acetic acid (99.8%) were obtained from MilliporeSigma (Burlington, USA). Multi-walled CNTs in a *N*,*N*-dimethylformamide (DMF) dispersion were received from XFNANO Materials Technology (Jiangsu, China). DMF, tetrahydrofuran (THF), ethanol, and acetone were bought from Beijing Yili Fine Chemical (Beijing, China). Sodium chloride (NaCl) was obtained from Sinopharm Chemical Reagents (Beijing, China). We also made up 0.9% NaCl solution and deionized water. All chemicals were of analytical grade and used as received without pretreatment.

Preparation of the Janus membrane

A piece of clean cotton gauze (5 cm × 5 cm) was immersed in a mixture of TMSPMA (4.75 mL) and acetic acid (0.25 mL). The reaction was conducted at 75 °C for 4 h under magnetic stirring followed by heating of the fabric at 105 °C for 24 h under a vacuum. Afterwards, the cotton gauze was extracted from the reaction solution and rinsed thrice with THF under shaking for 30 min each time. Then, a hydrophobic gauze (which we named "Hb-Gauze") was obtained after drying at 60 °C.

An electrospinning solution was prepared by dissolving sufficiently dried CA powder in a mixture of DMF and acetone (mass ratio = 2 : 1). After that, a DMF dispersion of multi-walled CNTs was added to the newly obtained solution so that the ratio became 20 wt% CA/0.5 wt% CNTs/DMF/acetone. After ultrasonic treatment for 1 h and magnetic stirring at room temperature for 8 h, a precursor solution was obtained. Then, Hb-Gauze was used as the substrate, which was covered on a rotating drum at a rotation speed of 200 rpm. After electrospinning, the Hb-Gauze/CNTs@CA Janus membrane was obtained. The distance and applied voltage of electrospinning

technology was set as 15 cm and 15 kV, respectively. The flow rate of the precursor solution was 0.08 mm min^{-1} and was controlled by an injection pump. In addition, electrospinning nozzles with inner diameters of 0.6, 0.8, 1.0, and 1.2 mm (named as 6G, 8G, 10G, and 12G, respectively) were equipped to obtain CNTs@CA fibrous membranes with different average fibre diameters. Meanwhile, the Hb-Gauze/CNTs@CA Janus membranes constructed with an average diameter of the CNTs@CA fibrous membrane of 0.6 mm and 1.2 mm were named "6G-Janus membrane" and "12G-Janus membrane", respectively.

Instruments and characterization

The surface morphologies of gauze, Hb-Gauze, electrospun CA, and CNTs@CA fibrous membranes were observed *via* a scanning electron microscope (JSM-6700; Tokyo, Japan). The fiber diameters of the above-mentioned samples were analyzed using image-analysis software provided by the scanning electron microscopy (SEM) system. Water contact angles (WCAs) were tested using a measurement system for WCAs (OCA 20; Data Physics, San Jose, USA). Deionized water droplets (5 μL) were dripped onto the membrane surface. The average WCA could be obtained by measuring at six different positions of the same sample. The chemical composition was tested and elemental distribution maps obtained using energy-dispersive X-ray spectroscopy (EDS) based on a Quanta 650FEG system (FEI, Hillsboro, USA). Fourier transform infrared (FTIR) spectroscopy of as-prepared samples was done using a FTIR spectrometer (Nicolet 8700, Madison, USA) in a wave range of 400 to 4000 cm^{-1}. X-ray photoelectron spectroscopy (XPS) using monochromatized Al Kα radiation ($h\nu = 1486.6$ eV, 225 W) as the X-ray source with a base pressure of 10^{-9} torr (AXIS Supra; Kratos, San Diego, USA) was used to analyze the surface chemical properties of fibrous membranes. The thickness of the CNTs@CA fibrous membrane was adjusted by fixing the area of the electrospinning substrate (5 cm × 5 cm) and then regulating the duration of electrospinning. A thickness gauge (CHY-U; Saicheng Instruments, Jinan, China) was used to measure the thicknesses of hybrid Janus membranes. The Xenon solar simulator (CEL-S500; Beijing China Education Au-light, Beijing, China) was used for indoor photothermal conversion, and the light intensity was 500 000 Lx.

Characterization of photothermal-conversion properties

All experiments were done at the Beijing Institute of Fashion Technology (Beijing, China). The heat-transfer properties of Janus membranes under irradiation by the Xenon solar simulator (indoor) and sunlight (outdoor) were characterized. Janus membranes of identical area (3 cm × 3 cm) were covered on k-type thermocouples (SA1XL-K; Omega Engineering, Norwalk, USA), and a laptop computer was used to record real-time temperature changes.

Permeability to water vapor

The rate of mass change of water vapor through a sample within a certain time was used as the standard to measure the moisture permeability of gauze, Hb-Gauze, 6G-Janus membrane, and 12G-Janus membrane. First, we cut samples into squares (5 cm × 5 cm) and fixed them on the mouth of a beaker filled with 10 mL of deionized water. Then, beakers covered with different samples were placed in the oven at 30 °C, 40 °C, or 60 °C. After 1 h, samples were removed and weighed, and their vapor-transmission rate (g m^{-2} h^{-1}) was calculated. Each sample was tested five times, and the average value was calculated as follows:

$$\text{Vapor-transmission rate} = \frac{M_0 - M_t}{tS}$$

where: M_0 and M_t represent the total mass of the sample covering the beaker before and after evaporation, respectively; $M_0 - M_t$ is the mass change of deionized water in the beaker before and after evaporation; S is the effective area of water vapor passing through the membrane composite membrane; t is the time.[43]

Results and discussion

The detailed fabrication process of a Janus membrane composed of TMSPMA grafted on a modified Hb-Gauze layer and a CNTs-doped CA fibrous layer is illustrated schematically in Fig. 1.

Initially, TMSPMA (which contains abundant silicon bonds) was chemically grafted on gauze. The hydroxyl groups on the surface of pristine cotton gauze could be replaced, which ensured that the gauze changed from exhibiting super-hydrophilicity to hydrophobicity.[44] After that, CNTs were dispersed in the CA electrospinning precursor solution by strong ultrasonic treatment. Then, hydrophilic CNTs-doped CA fibers (CNTs@CA) were obtained by electrospinning, and stacked on Hb-Gauze seamlessly to form a Hb-Gauze/CNTs@CA Janus membrane with asymmetric wettability. To further explore the influence of the TMSPMA amount on wettability, the relationship between the TMSPMA concentrations and WCAs are provided in Table S1 and Fig. S1 in ESI.† As the TMSPMA concentration increased, the WCA changed within 10°, indicating that the wettability of the Hb-Gauze showed no obvious change with the TMSPMA concentration. SEM was used to ascertain if the morphologies of the yarns surface had changed after TMSPMA modification. The SEM images of pristine gauze, Hb-Gauze-95%, and Hb-Gauze-45% are shown in Fig. 2a. All these gauzes were reticular and consisted of interwoven bundles of yarns. Meanwhile, the TMSPMA concentration had no effect on the surface morphology of gauzes. Combined with the WCA results in Fig. S1 (ESI†), the TMSPMA concentration was 95%. Hb-Gauze-95% was chosen for further research and was named "Hb-Gauze". EDS was used to analyze the elements and their distributions in gauze (Fig. 2b) and Hb-Gauze (Fig. 2c). According to Fig. 2b, the pristine cotton gauze mainly contained C (53.45 wt%) and O (46.55 wt%) elements. For Hb-Gauze, besides C and O elements, Si was detected. The corresponding amount of C, O, and Si (in wt%) was 51.58, 42.22, and 6.21, respectively. For the hydrophilic CNTs@CA electrospun fibrous layer, the electrospinning conditions of CA fibrous membranes

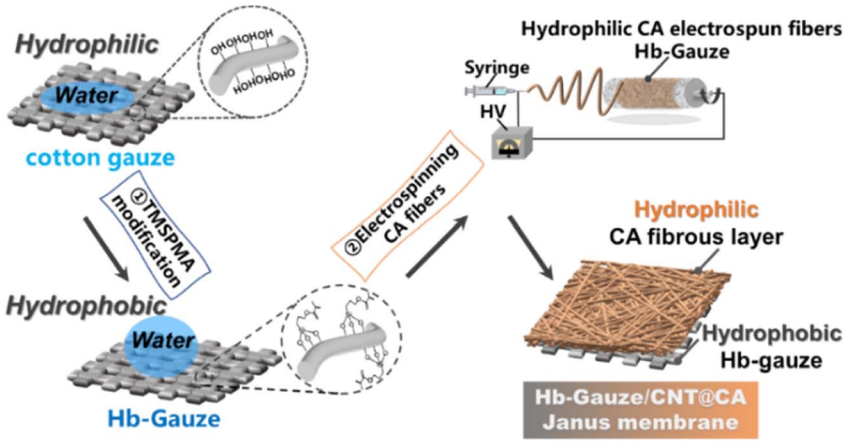

Fig. 1 Fabrication of a Hb-Gauze/CNTs@CA Janus fibrous membrane (schematic).

were explored initially. Fig. 2d shows the SEM images of electrospun CA fibrous membranes fabricated with different concentrations of CA solution. With an increase in the concentration of the electrospun CA solution from 12.5 wt% to 20 wt%, the corresponding morphology of CA changed from spheres, knot-in-fiber structures, to smooth and uniform fibers gradually. The WCA of corresponding samples are shown in Fig. S2 (ESI†). Compared with other samples, the CA fibrous membrane electrospun with a solution concentration of 20 wt% exhibited uniform fibrous morphology, but also had the lowest WCA (*i.e.*, more hydrophilicity). We also electrospun CA fibrous membranes with different inner diameters of the nozzle and concentration of CA solution of 20 wt%. The WCA improved with increasing of the inner diameter of nozzles (Fig. S2, ESI†). Considering morphological uniformity and excellent hydrophilicity, we chose a concentration of CA electrospinning solution of 20 wt% in subsequent studies.

Afterwards, CNTs were doped into CA electrospinning solution to enhance hydrophilicity and increase the thermal-conversion capacity of the CA fibrous membrane. To obtain

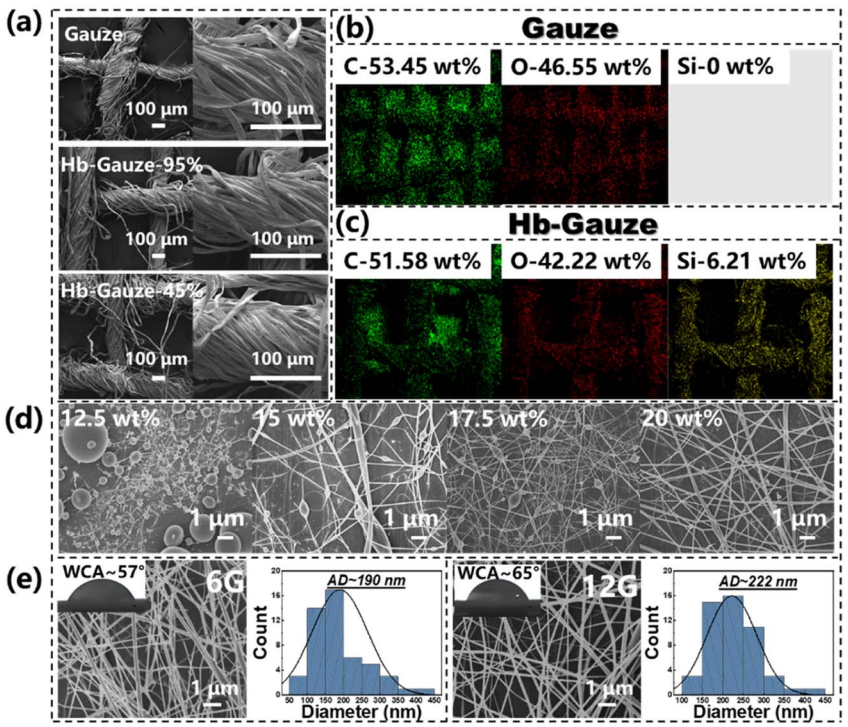

Fig. 2 Morphology and chemical analysis of prepared membranes. (a) SEM images of pristine gauze, Hb-Gauze-95%, and Hb-Gauze-45%. (b and c) Element-distribution maps of gauze and Hb-Gauze according to EDS. (d) SEM images of a CA fibrous membrane electrospun with different solution concentrations. (e) SEM images, statistic average fiber diameters, and water contact angles corresponding to CA-doped (20 wt%) CNTs (0.5 wt%) with 6G and 12G electrospinning nozzles, respectively.

fibers with a large difference in mean diameter, the electrospun nozzle types of 6G and 12G (which had the smallest and largest inner diameter of nozzles, respectively) were used in fabrication of the CNTs@CA fibrous membrane. In this way, we explored the influence of the maximum morphology of the fibrous membrane on wet and thermal management. SEM images of CNTs@CA fibrous membranes electrospun with 6G and 12G are shown in Fig. 2e. The WCA before and after doping CNTs is shown in Fig. S3 (ESI†). The WCA of the CA electrospun fibrous membrane was ~80°. After doping of CNTs, the WCA decreased to ~55°, indicating that CNTs-doping increased the hydrophilicity of the CA electrospun fibrous membrane. Furthermore, with an increasing inner diameter of the nozzle (*i.e.*, from 6G to 12G), the corresponding average diameter of CNTs@CA fibers increased from 190 nm to 222 nm, and the WCA increased from 57° to 65°. In addition, the CNTs@CA membrane was observed by TEM (Fig. S4, ESI†). The doped CNTs were "wrapped" in CA fibers and present in large quantities in the fiber membrane. The FTIR spectra of CA and CNTs@CA membrane are shown in Fig. S5 (ESI†). A C=C stretching vibration peak appearing at 1650 cm^{-1} of the CNTs@CA fibrous membrane could be attributed to sp^2 hybridization of the carbon–carbon double bonds in CNTs.[45] These phenomena indicated that CNTs were well doped.

Fig. 3 provides the FTIR and XPS spectra of gauze and Hb-Gauze. According to the FTIR spectra in Fig. 3a, compared with gauze, the peak of Hb-Gauze at 1727 cm^{-1} changed slightly, which was attributed to the vibration of O–C=O connected to Si groups.[46] Meanwhile, the stretching vibration peak at 799 cm^{-1} arose from Si–C, which also indicated TMSPMA had been modified on cotton gauze.[47] The full spectra of XPS for gauze and Hb-Gauze are shown in Fig. 3, and indicated that gauze contained C and O elements, and Hb-Gauze contained C, O, and Si elements. Fig. 3c shows the high-resolution XPS C 1s spectra of gauze. Peaks located at ~284 eV, ~286 eV, and ~288 eV were assigned to C–O, C–C, and C=O, respectively. For Hb-Gauze, peaks located at ~284 eV, ~285 eV, ~289 eV, and ~289 eV could be assigned to C–O, Si–C, C–C, and C=O, respectively (Fig. 3d). The high-resolution XPS O 1s spectra of cotton gauze showed peaks located at ~532 and ~535 eV, which could be assigned to C–O and C=O groups. The high-resolution XPS O 1s spectra of Hb-Gauze showed peaks located at ~532 eV, ~533 eV, and ~534 eV, which were assigned to C–O, Si–O, and C=O, groups, respectively. As a result of electronic spin–orbit coupling, the Si 2p of Hb-Gauze in the spectra showed peaks located at ~101 and ~103 eV, which were assigned to Si–O and Si–C groups. These data further confirmed that TMSPMA had been modified on gauze. Fig. 3e describes (schematically) the change in chemical groups before and after TMSPMA modification. After chemical modification by TMSPMA, the hydroxyl groups on the gauze surface were replaced by methoxysilane. Such methoxysilane enabled construction of a stable hydrophobic –Si–O–C– structure on the surface of the gauze, which made the modified gauze exhibit excellent hydrophobicity.[48]

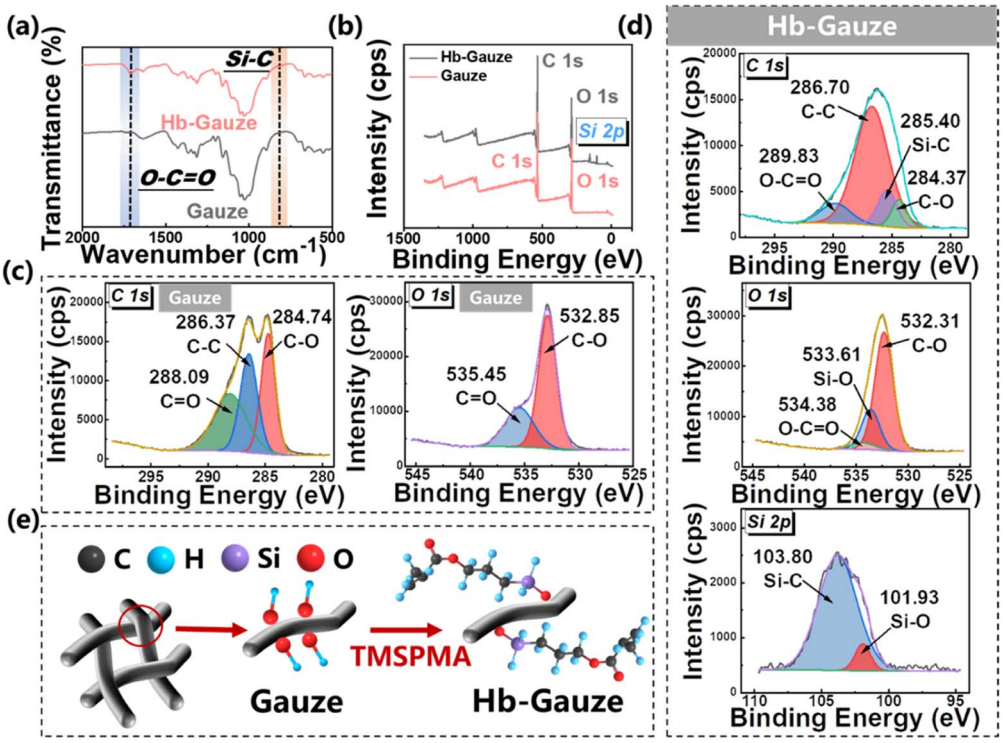

Fig. 3 FTIR spectroscopy and XPS of Janus membranes. (a) FTIR spectra of gauze and Hb-Gauze. (b) Full XPS survey spectra of gauze and Hb-Gauze. (c) High-resolution XPS spectra of C 1s and O 1s peaks of gauze. (d) High-resolution XPS spectra of C 1s, O 1s, and Si 2p peaks of Hb-Gauze. (e) Molecular compositions of gauze and Hb-Gauze during modification (schematic).

The capacity for sweat/moisture transport is very important for wetness regulation. In our previous works, Janus membranes had a novel capacity for unidirectional liquid transport. Hence, liquid could be transported from one side to the other side unidirectionally but was blocked from the reverse side.[49–51] Such a unique capacity for unidirectional liquid transport endows a great potential to expel sweat/moisture from human skin efficiently.[52] Nonetheless, different Janus membranes have different layouts for hydrophobic/hydrophilic combination. Hence, not all Janus membranes exhibit the capability of unidirectional liquid transport.[53] Therefore, the thickness of the hydrophilic layer of the CNTs@CA fibrous membrane must be adjusted by changing the electrospinning duration (that is, exploration of the synergistic effect of the hydrophobic/hydrophilic layer on the capacity for unidirectional liquid transport of the Janus membrane). CNTs@CA fibrous membranes were electrospun on the Hb-Gauze substrate with 6G and 12G, respectively, and the obtained Janus membranes were named "6G-Janus" and "12G-Janus", respectively. The relationship between the 6G-Janus membrane and 12G-Janus membrane with respect to the duration of CNTs@CA electrospinning and thickness is shown in Table S2 (ESI†). The thickness of 6G- and 12G-Janus membranes increased with prolonged electrospinning. The thickness of the 12G-Janus membrane increased more obviously. Fig. 4a shows real-life liquid (0.9% saline solution to simulate sweat and moisture from the human body) transport of the 12G-Janus membrane. When the liquid dropped on the hydrophobic Hb-Gauze layer, the liquid drop maintained its original state on the hydrophobic layer. Until the amount of liquid increased, it penetrated and made contact with the hydrophilic of layer CNTs@CA. After that, the liquid drop gradually transported unidirectionally from the hydrophobic layer to the hydrophilic layer under the action of capillary force (CF), thereby penetrating the entire Janus membrane. When the liquid dropped on the hydrophilic layer, it could not penetrate downwards, but instead diffused on the hydrophilic layer, causing unidirectional liquid transport.

As displayed in Fig. 4b, the electrospinning duration of the 6G-Janus membrane had to be >20 min to achieve unidirectional liquid transport. If the electrospinning duration was >55 min, due to the increased thickness of the CNTs@CA hydrophilic layer, unidirectional liquid transport could not be achieved. For the 12G-Janus membrane, the electrospinning duration had to be 35–75 min to realize unidirectional liquid transport. We wished to further explore the effect of the thickness of hydrophilic CNTs@CA on liquid transport. The relationship between the maximum height of a water column that fibrous membranes could support before water passed through them (*i.e.*, hydrostatic pressure (HP)) and duration of unidirectional liquid transport was explored. In general, the HP of the two Janus membranes from the hydrophilic layer to the

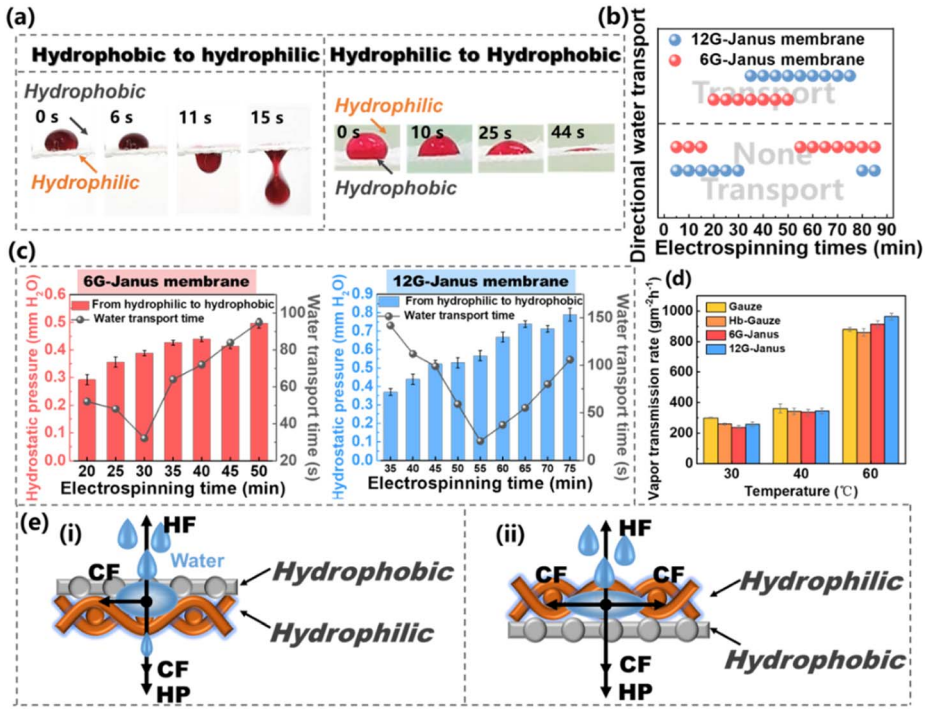

Fig. 4 Unidirectional liquid transport of Janus membranes. (a) Real-time unidirectional liquid transport of the Janus membrane when liquid was dropped on its hydrophobic layer and in the reverse direction. (b) Relationship between liquid-transport performances of a series of Janus membranes prepared with different electrospinning nozzles and thickness of hydrophilic CNTs@CA adjusted by electrospinning duration. (c) Relationship between HP and electrospinning duration of the hydrophilic CNTs@CA of the Janus membrane and water-transmission rate from the hydrophobic layer to the hydrophilic layer. (d) Moisture vapor transmission rate of the 6G-Janus membrane, 12G-Janus membrane, Hb-Gauze, and gauze at different temperatures. (e) Unidirectional liquid transport of the Hb-Gauze/CNTs@CA Janus membrane.

hydrophobic layer increased with increasing duration of electrospinning, whereas the time taken for liquid to be transported from the hydrophobic layer to the hydrophilic layer decreased and then increased (Fig. 4c). This phenomenon was due to the increase in electrospinning duration, which led to an increased thickness of the Janus membrane and hindered penetration of the liquid through the entire Janus membrane. However, the time taken for the liquid to be transported decreased and then increased because the thickness of the hydrophilic layer increased the CF, which helped the liquid to pass through the Janus membrane. However, as the thickness continued to increase, the increased CF was not sufficient to offset the negative effect of membrane thickness. Therefore, the time taken for the liquid to be transported decreased first and then increased. When the electrospinning duration of the 6G-Janus membrane was 30 min, the time taken for the liquid to be transported was the fastest and the HP was low. For the 12G-Janus membrane, when the electrospinning duration was 55 min, the time taken for the liquid to be transported was the fastest, and the HP transformation was low. Thus, the 6G-Janus membrane with an electrospinning duration of 30 min and the 12G-Janus membrane with an electrospinning duration of 55 min were chosen as the optimal electrospinning durations for further research.

Besides unidirectional liquid transport, the moisture-vapor transport rate (MVTR) of the Janus membrane at different temperatures was explored by weighing the mass loss of water before (M_0) and after (M_t) heating per unit per hour (Fig. 4d). Fig. 4d shows the MVTR of gauze, Hb-Gauze, 6G-Janus membrane, and 12G-Janus membrane at different temperatures. At 30 °C, the MVTR of pristine gauze and Hb-Gauze was slightly higher than that of the Janus membranes. When the temperature increased to 40 °C, the MVTR of gauze and Hb-Gauze remained higher than that of the Janus membrane, but the MVTR growth was lower than that of the two Janus membranes, which resulted from the unidirectional liquid transport of the Janus membranes. At 60 °C, the MVTR of the two kinds of Janus membranes was higher than that of gauze and Hb-Gauze. When moisture vapor encountered a hydrophobic layer, it was captured and transported from the hydrophobic layer to the hydrophilic layer, and this effect was more pronounced at high temperatures. Moreover, the moisture vapor transported from the hydrophobic layer barely soaked the Janus membrane, allowing the dry hydrophobic side to continuously trap tiny droplets and continued to speed up liquid transport. To demonstrate the mechanism of wet management of the Hb-Gauze/CNTs@CA Janus membrane, based on unidirectional liquid transport, simple physical models were established. When the liquid first made contact with the surface of the hydrophobic layer of Hb-Gauze, the hydrophobic layer could produce hydrophobic force (HF) resistance to the liquid, and the liquid itself produced HP against this resistance.[54–56] With an increase in the amount of liquid, the HP would increase and the liquid would infiltrate. When the liquid came into contact with hydrophilic CNTs@CA fibers, another CF was generated which, in combination with, HP, helped the liquid to continue to permeate, eventually allowing the liquid to penetrate the entire Janus membrane.[57,58] However, when the liquid first made contact with the surface of the hydrophilic layer of CNTs@CA, there was strong wicking behavior due to the combined effect of CF and HP, which caused the liquid to spread across the surface.[59–61] Therefore, the Janus membrane with asymmetric wettability and unidirectional wicking achieved novel unidirectional liquid transport.

CNTs have an ultra-wide band-absorption spectrum and a pure black appearance, which permits excellent light absorption.[62] As a result, CNTs have strong photothermal-conversion capacity, which can reduce energy consumption and be applied in the thermal management of textiles or fabrics to improve personal thermal comfort. The photothermal-conversion capacity of prepared membranes under indoor (irradiation from a xenon lamp) and outdoor (irradiation by sunlight) conditions were investigated, respectively (Fig. 5a and b). The distance between the xenon lamp and sample was 20 cm during measurement. As shown in Fig. 5a, the highest temperature that the 12G-Janus membrane reached was ~87 °C after 500 s of xenon-lamp irradiation, which was slightly higher than that of the 6G-Janus membrane (~81 °C) and much higher than that of gauze (~74 °C), Hb-Gauze (~75 °C) as well as ambient temperature (~39 °C). The temperature reached by the 6G-Janus membrane and 12G-Janus membrane was ~12 °C and ~6 °C higher than that reached by Hb-Gauze, respectively, indicating that the 12G-Janus membrane exhibited better heat-collection performance than that of the 6G-Janus membrane. Meanwhile, on a sunny day (9 July, 2022 in Beijing, China), we conducted a photothermal-conversion experiment outdoors from 9:30 AM to 5:30 PM (Fig. 5b). In general, the temperature curves of all membranes fluctuated due to wind gusts. The highest temperature reached by the 12G-Janus membrane was ~61 °C at noon, which was much higher than the temperature of the environment (~46 °C), 6G-Janus membrane (~56 °C), and Hb-Gauze (~52 °C). Then, we used infrared thermal imaging to obtain more intuitive data of effects of thermal management. Images of temperature variation during moisture transport are provided in Fig. 5c. The 12G-Janus membrane, 6G-Janus membrane, and Hb-Gauze were covered on a wetted arm. Images were taken *via* an infrared camera after 20 s. When the hydrophobic side stuck to skin, the temperature of the 12G-Janus membrane and 6G-Janus membrane was higher than that of Hb-Gauze. Hence, heat produced by the human body was transported from the epidermis to the environment during unidirectional transport of sweat/moisture. When the hydrophilic side stuck to skin, the temperature of the 12G-Janus membrane and 6G-Janus membrane was lower than that of Hb-Gauze. These results indicated that, when the hydrophilic CNTs@CA fibrous layer faced the external environment, the excellent photothermal-conversion capacity of CNTs endowed outstanding heat-collection capacity. Besides, the Janus membrane drove sweat/moisture to the external environment but also carried some heat away from the surface of human skin. That is, a synergistic effect of wet–thermal management was realized. When the hydrophobic layer faced the external

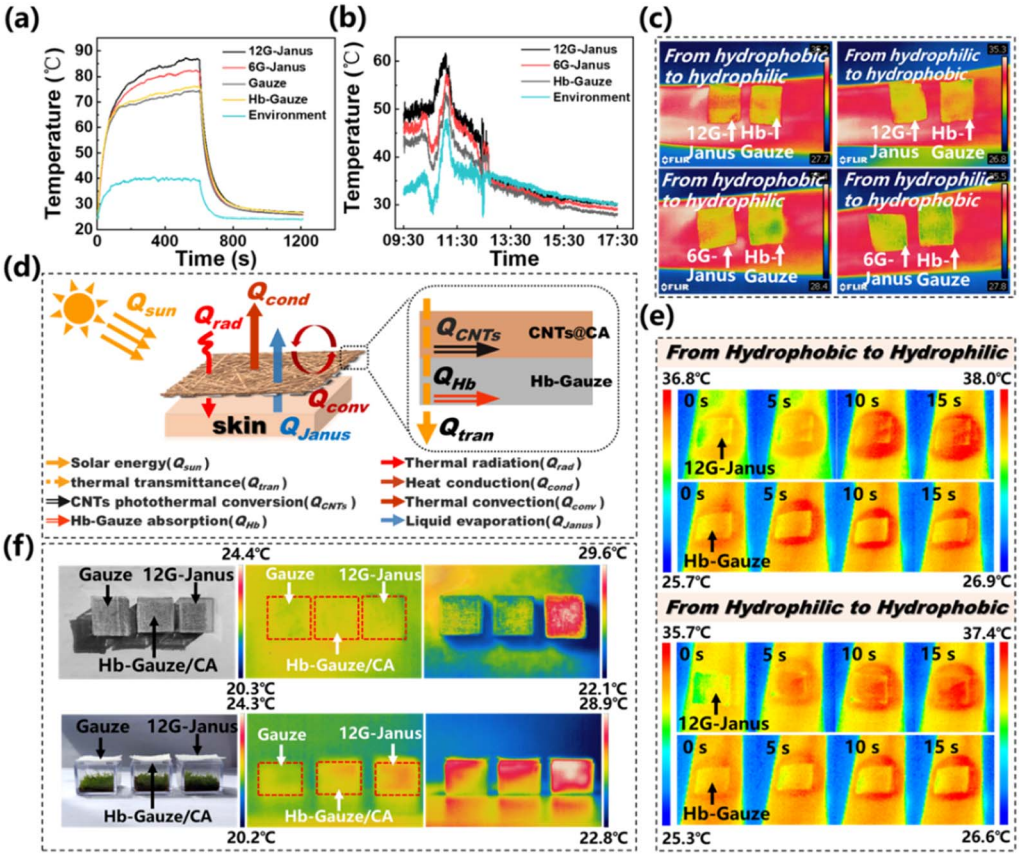

Fig. 5 Characterization of photothermal conversion. (a) Temperature variations of different fibrous membranes indoors under xenon-lamp irradiation. (b) Temperature variations of different fibrous membranes outdoors on sunny days. (c) The 12G-Janus membrane or 6G-Janus membrane were placed on moist human skin together with Hb-Gauze and photographed with an infrared camera. (d) Heat conduction of Hb-Gauze/CNTs@CA Janus membranes (schematic). (e) Under xenon-lamp irradiation, the two sides of the 12G-Janus membrane were compared with infrared thermal images of Hb-Gauze placed on human skin. (f) Gauze, Hb-Gauze/CA, and 12G-Janus were covered in small boxes of green plants, and infrared cameras used to photograph their appearance above and on the front in the sun.

environment, heat transfer was reduced so that the temperature of the Janus membrane was the same as that of Hb-Gauze.

Based on the data stated above, a heat-transfer mechanism of the Hb-Gauze/CNTs@CA Janus membrane was postulated (Fig. 5d). In the human skin–fibrous fabric–external environment, the heat Q obtained by the whole system can be expressed as:

$$Q = Q_{rad} + Q_{sun} - Q_{conv} - Q_{cond} - Q_{Janus} \quad (1)$$

where Q_{conv} and Q_{cond} is the heat loss due to thermal convection and thermal conduction, respectively; Q_{Janus} is the heat loss by the Janus structure for efficient liquid evaporation; Q_{rad} and Q_{sun} denote the whole system that can absorb heat. The heat from the sun can be interpreted as:

$$Q_{sun} = Q_{CNTs} + Q_{Hb} + Q_{tran} \quad (2)$$

where Q_{CNTs} is the heat generated by solar photothermal conversion of CNTs; Q_{Hb} is the heat absorbed by Hb-Gauze; Q_{tran} is the thermal transmittance. In general, the Q_{cond} from a human to the system is basically identical because the body temperature is unchanged essentially. The factors influencing Q_{conv} are the surface temperature and external environment. Although the surface temperature of fibrous membranes is different, it has little effect on the whole system. Therefore, Q_{rad}, Q_{sun} and Q_{Janus} affect the different heat obtained by fabrics.

For the Hb-Gauze/CNTs@CA Janus membrane, the doped CNTs improved the photothermal-conversion efficiency and increased Q_{rad} and Q_{CNTs}. The Janus structure resulted in unidirectional liquid transport, so part of the heat would be taken away when sweat/moisture was transported to the external environment, causing heat loss of the system (Q_{Janus}). Albeit, the Q_{tran} of Hb-Gauze was higher than that of the Janus membrane due to its large aperture, it is was not enough to offset the gap between the Q_{rad} and Q_{CNTs}. Therefore, the temperature of the Hb-Gauze/CNTs@CA Janus membrane was higher than that of Hb-Gauze.

We found that the thermal management of the 12G-Janus membrane was better than that of the 6G-Janus membrane in indoor and outdoor environments. Therefore, we chose the 12G-Janus membrane and gauze to cover skin and, through heating from a xenon lamp, used an infrared camera to observe the entire heating process. According to Fig. 5e, when the

hydrophilic layer (which contained CNTs) faced upwards, the temperature of the 12G-Janus membrane was higher than that of Hb-Gauze after 15 s of radiation by the xenon lamp. In comparison, when the hydrophobic layer faced upwards, although the temperature of the 12G-Janus membrane was higher than that of Hb-Gauze eventually, the rate of temperature increase of the 12G-Janus membrane was slower.

Furthermore, we placed Hb-Gauze, Hb-Gauze/CA, and 12G-Janus on three transparent and uncapped boxes in sunlight, respectively (Fig. 5f). The infrared camera revealed that the surface temperature of the 12G-Janus membrane was significantly higher than that of Hb-Gauze and Hb-Gauze/CA under irradiation by sunlight. In addition, observation within an enclosed space revealed the heating effect of the 12G-Janus membrane to be improved significantly in the whole space. Hence, the 12G-Janus membrane could be used for heating of indoor spaces, which could take advantage of solar energy for stable wet–thermal management.

Conclusions

Using a combination of chemical modification and electrospinning, an asymmetric wettability Hb-Gauze/CNTs@CA Janus membrane with excellent heat-collection properties and unidirectional liquid transport was obtained. Compared with bare skin, covering the Hb-Gauze/CNTs@CA Janus membrane could increase the skin temperature by 10 °C. This Janus membrane could offer unidirectional liquid transport so that it removed sweat quickly and kept skin dry. The Janus membrane could keep the human body at the correct temperature in a cold climate, and export sweat to the surface of human skin. This phenomenon could make fabric more comfortable when working or living in cold conditions. We anticipate that this work could: (i) provide new ideas for the design and manufacture of fabrics with excellent heat collection and sweat/moisture permeability; (ii) expand the application prospects of this Janus membrane in personal wet–thermal management. Our developed Janus membrane has broad development prospects in "smart" wearable textiles.

Author contributions

J. Wu had the original idea and designed the experiments. B. Tian carried out the experiments and analyzed experimental data. M. Hu and Y. Yang helped to analyze data. J. Wu guided the study, and wrote and revised the manuscript.

Conflicts of interest

The authors declare no conflicts of interest.

Acknowledgements

The authors acknowledge the National Science Foundation of China (21503005), Beijing Municipal Natural Science Foundation (2154047), Youth Outreach Project of Beijing (CIT&TCD201904058), Youth Outreach Project of Beijing Institute of Fashion Technology (BIFTBJ201806), Beijing Scholars Program (RCQJ20303), R&D Program of Beijing Municipal Education Commission (KM202310012001), 2023 Graduate Research Innovation Project of Beijing Institute of Fashion Technology (NHFZ20230067), and High-Level Scientific Research Project of Cultivation Foundation of Beijing Institute of Fashion Technology.

Notes and references

1 A. K. Melikov, *Indoor Air*, 2004, **14**, 157–167.
2 X. Yue, T. Zhang, D. Yang, F. Qiu, G. Wei and H. Zhou, *Nano Energy*, 2019, **63**, 103808.
3 S. B. Sadineni, S. Madala and R. F. Boehm, *Renewable Sustainable Energy Rev.*, 2011, **15**, 3617–3631.
4 L. Cai, A. Song, P. Wu, P. Hsu, Y. Peng, J. Chen, C. Liu, P. Catrysse, Y. Liu, A. Yang, C. Zhou, C. Zhou, S. Fan and Y. Cui, *Nat. Commun.*, 2017, **8**, 496.
5 P. Hsu, A. Song, P. Catrysse, C. Liu, Y. Peng, J. Xie, S. Fan and Y. Cui, *Science*, 2016, **353**, 1019–1023.
6 G. L. Stephens, B. H. Kahn and M. Richardson, *J. Clim.*, 2016, **29**, 5469–5482.
7 Y. Cao, S. Liang, X. Chen, T. He, D. Wang and X. Cheng, *Sci. Rep.*, 2017, **7**, 8462.
8 R. Hu, Y. Liu, S. Shin, S. Huang, X. Ren, W. Shu, J. Cheng, G. Tao, W. Xu, R. Chen and X. Luo, *Adv. Energy Mater.*, 2020, **10**, 1903921.
9 Y. Peng and Y. Cui, *Joule*, 2020, **4**, 723–742.
10 M. Shen, J. Ni, Y. Cao, Y. Yang, W. Wang and J. Wang, *J. Mater. Sci. Technol.*, 2023, **133**, 32–40.
11 J. McCorriston, *Curr. Anthropol.*, 1997, **38**, 517–535.
12 R. G. Lipsey, *J. Inst. Econ.*, 2009, **5**, 259–288.
13 L. Lei, S. Shi, D. Wang, S. Meng, J. Dai, S. Fu and J. Hu, *ACS Nano*, 2023, **17**, 1803–1830.
14 V. Correia, T. Stephenson and S. Judd, *Environ. Technol.*, 1994, **15**, 917–929.
15 J. Zhang, J. Ge, Y. Si, F. Zhang, J. Yu, L. Liu and B. Ding, *Nanoscale Horiz.*, 2019, **4**, 1174–1184.
16 S. Lomov, G. Huysmans, Y. Luo, R. Parnas, A. Prodromou, I. Verpoest and F. Phelan, *Composites, Part A*, 2001, **32**, 1379–1394.
17 K. Jost, G. Dion and Y. Gogotsi, *J. Mater. Chem. A*, 2014, **2**, 10776–10787.
18 H. Woo, K. Zhou, S. Kim, A. Manjarrez, M. Hoque, T. Seong and L. Cai, *Adv. Funct. Mater.*, 2022, **32**, 2201432.
19 J. Wu, M. Zhang, M. Su, Y. Zhang, J. Liang, S. Zeng, B. Chen, L. Cui, C. Hou and G. Tao, *Adv. Fiber Mater.*, 2022, **4**, 1545–1555.
20 R. Cheng, B. Wang, J. Zeng, J. Li, J. Xu, W. Gao and K. Chen, *ACS Appl. Mater. Interfaces*, 2022, **14**, 30144–30159.
21 S. Chen, Z. Li, J. Huang, L. Sha and Z. Lu, *Chem. Eng. J.*, 2023, **457**, 141021.
22 C. Liang, J. He, Y. Zhang, W. Zhang, C. Liu, X. Ma, Y. Liu and J. Gu, *Compos. Sci. Technol.*, 2022, **224**, 109445.
23 S. Iijima, *Nature*, 1991, **354**, 56–58.
24 A. M. Marconnet, M. A. Panzer and K. E. Goodson, *Rev. Mod. Phys.*, 2013, **85**, 1295–1326.

25 A. A. Balandin, *Nat. Mater.*, 2011, **10**, 569–581.
26 P. Kim, L. Shi, A. Majumdar and P. L. McEuen, *Phys. Rev. Lett.*, 2001, **87**, 215502.
27 M. Fujii, X. Zhang, H. Xie, H. Ago, K. Takakhashi, T. Ikuta, H. Abe and T. Shimizu, *Phys. Rev. Lett.*, 2005, **95**, 065502.
28 X. Xu, J. Chen, J. Zhou and B. Li, *Adv. Mater.*, 2018, **30**, 1705544.
29 D. Hu, L. Han, W. Zhou, P. Li, Y. Huang, Z. Yang and X. Jia, *Chem. Eng. J.*, 2022, **437**, 135056.
30 Y. Chen, B. Zhao, H. Zhang, T. Zhang, T. Zhang, D. Yang and F. Qiu, *Chem. Eng. J.*, 2022, **450**, 138177.
31 F. Zhang, Y. Feng, M. Qin, T. Ji, F. Lv, Z. Li, L. Gao, P. Long, F. Zhao and W. Feng, *Carbon*, 2019, **145**, 378–388.
32 H. Wang, A. S. Tazebay, G. Yang, H. T. Lin, W. Choi and C. Yu, *Carbon*, 2016, **106**, 152–157.
33 Q. Liu, J. Huang, J. Zhang, Y. Hong, Y. Wan, Q. Wang, M. Gong, Z. Wu and C. Guo, *ACS Appl. Mater. Interfaces*, 2018, **10**, 2026–2032.
34 C. Wang, K. Xia, Y. Zhang and D. Kaplan, *Acc. Chem. Res.*, 2019, **52**, 2916–2927.
35 Z. Shao and F. Vollrath, *Nature*, 2002, **418**, 741.
36 B. Zhu, W. Li, Q. Zhang, D. Li, X. Liu, Y. Wang, N. Xu, J. Li, X. Li, P. B. Catrysse, W. Xu, S. Fan and J. Zhu, *Nat. Nanotechnol.*, 2021, **16**, 1342–1348.
37 R. S. Hale, R. Ranjan and C. H. Hidrovo, *Int. J. Heat Mass Transfer*, 2014, **75**, 710–717.
38 Y. Gu, J. Wu, M. Hu, H. Pi, R. Wang and X. Zhang, *RSC Adv.*, 2022, **12**, 32–41.
39 L. Lao, D. Shou, Y. Wu and J. Fan, *Sci. Adv.*, 2020, **6**, eaaz0013.
40 L. Yan, X. Yang, Y. Zhang, Y. Wu, Z. Cheng, S. B. Darling and L. Shao, *Mater. Today*, 2021, **51**, 626–647.
41 H. Zhou and Z. Guo, *J. Mater. Chem. A*, 2019, **7**, 12921–12950.
42 D. Miao, Z. Huang, X. Wang, J. Yu and B. Ding, *Small*, 2018, **14**, 1801527.
43 R. L. Kovács, L. Daróczi, P. Barkóczy, E. Baradács, E. Bakonyi, S. Kovács and Z. Erdályi, *J. Coat. Technol. Res.*, 2021, **18**, 523–534.
44 Y. Wang, X. Liang, H. Zhu, J. H. Xin, Q. Zhang and S. Zhu, *Adv. Funct. Mater.*, 2020, **30**, 1907851.
45 X. Zheng, W. Xu and S. Xie, *Materials*, 2021, **14**, 5672.
46 S. Wu, W. Xu, F. Zhang and H. Wu, *Coatings*, 2022, **12**, 590.
47 H. Sun, X. Liu, H. Yan, Z. Feng, B. Yu, N. Ning, M. Tian and L. Zhang, *Polymer*, 2019, **165**, 1–10.
48 C. Goussé, H. Chanzy, G. Excoffier, L. Soubeyrand and E. Fleury, *Polymer*, 2002, **43**, 2645–2651.
49 M. Hu, J. Wu, B. Tian, H. Pi, R. Wang and X. Zhang, *ACS Appl. Nano Mater.*, 2022, **5**, 7344–7356.
50 J. Wu, H. Zhou, H. Wang, H. Shao, G. Yan and T. Lin, *Adv. Mater. Interfaces*, 2019, **6**, 1801529.
51 B. Ren, H. Pi, X. Zhao, M. Hu, X. Zhang, R. Wang and J. Wu, *Nanoscale*, 2021, **13**, 9352–9363.
52 Y. Wang, G. Yue, D. Li, L. Hou, X. Zhao, Z. Cui, J. Bai, N. Wang and Y. Zhao, *Macromol. Rapid Commun.*, 2020, **41**, 2000089.
53 S. Tang, H. Pi, Y. Zhang, J. Wu and X. Zhang, *Appl. Sci.*, 2019, **9**, 3302.
54 J. Wu, N. Wang, L. Wang, H. Dong, Y. Zhao and L. Jiang, *Soft Matter*, 2012, **8**, 5996.
55 Z. Zhao, Y. Ning, S. Ben, X. Zhang, Q. Li, C. Yu, X. Jin, K. Liu and L. Jiang, *Adv. Sci.*, 2022, **9**, 2103765.
56 Z. Wang, J. Yang, X. Dai, J. Guo, S. Li, T. Sherazi and S. Zhang, *J. Membr. Sci.*, 2021, **627**, 119229.
57 H. Pi, Y. Xi, J. Wu, M. Hu, B. Tian, Y. Yang, R. Wang and X. Zhang, *Chem. Eng. J.*, 2023, **455**, 140853.
58 H. Chi, Z. Xu, Z. Wei, T. Zhang, T. Lin and Y. Zhao, *ACS Appl. Mater. interfaces*, 2021, **13**, 29150–29157.
59 H. Zhou, H. Wang, T. Lin and H. Niu, *Chem. Eng. J.*, 2022, **427**, 131936.
60 L. Hou, N. Wang, X. Man, Z. Cui, J. Wu, J. Liu, S. Li, Y. Gao, D. Li, L. Jiang and Y. Zhao, *ACS Nano*, 2019, **13**, 4124–4132.
61 R. Hu, N. Wang, L. Hou, Z. Cui, J. Liu, D. Li, Q. Li, H. Zhang and Y. Zhao, *J. Mater. Chem. A*, 2019, **7**, 124.
62 W. Yu, C. Liu and S. Fan, *Nano Res.*, 2021, **14**, 2471–2490.